Atmos. Chem. Phys. Discuss., https://doi.org/10.5194/acp-2018-332
Manuscript under review for journal Atmos. Chem. Phys.
Discussion started: 22 May 2018

Atmospheric Chemistry and Physics Discussions

Long-range transport of volcanic aerosol from the 2010 Merapi tropical eruption to Antarctica

Xue Wu[1,2], Sabine Griessbach[1], Lars Hoffmann[1]

[1]Jülich Supercomputing Centre, Forschungszentrum Jülich, Jülich, Germany
[2]Key Laboratory of Middle Atmosphere and Global Environment Observation, Institute of Atmospheric Physics, Chinese Academy of Sciences, Beijing, China

Correspondence to: Xue Wu (xu.wu@fz-juelich.de)

Abstract

Volcanic sulfate aerosol is an important source of sulfur for Antarctica where other local sources of sulfur are rare. Mid- and high latitude volcanic eruptions can directly influence the aerosol budget of the polar stratosphere. However, tropical eruptions can also enhance polar aerosol load following long-range transport. In the present work, we analyze the volcanic plume of a tropical eruption, Mount Merapi in October 2010, using the Lagrangian particle dispersion model Massive-Parallel Trajectory Calculations (MPTRAC), Atmospheric Infrared Sounder (AIRS) SO_2 observations and Michelson Interferometer for Passive Atmospheric Sounding (MIPAS) aerosol observations. We investigate the pathway and transport efficiency of the volcanic aerosol from the tropical tropopause layer (TTL) to the lower stratosphere over Antarctica. We first estimated the time- and height-resolved SO_2 injection time series over Mount Merapi during the explosive eruption using the AIRS SO_2 observations and a backward trajectory approach. Then the SO_2 injections were tracked for up to 6 months using the MPTRAC model. The Lagrangian transport simulation of the volcanic plume was compared to MIPAS aerosol observations and showed good agreement. Both of the simulation and the observations presented in this study suggest that a significant amount of aerosols of the volcanic plume from the Merapi eruption was transported from the tropics to the south of 60°S within one month after the eruption and even further to Antarctica in the following two months. This relatively fast meridional transport of volcanic aerosol was mainly driven by quasi-horizontal mixing from the TTL to the extratropical lower stratosphere, which was facilitated by the weakening of the subtropical jet during the seasonal transition from austral spring to summer and linked to the westerly phase of the quasi-biennial oscillation (QBO). When the plume went to southern high latitudes, the polar vortex was displaced from the south pole, so the volcanic plume was carried to the south pole without penetrating the polar vortex. Based on the model results, the most efficient pathway for the quasi-horizontal mixing was in between the isentropic surfaces of 360 and 430 K. Although only 4% of the initial SO_2 load was transported into

Atmos. Chem. Phys. Discuss., https://doi.org/10.5194/acp-2018-332
Manuscript under review for journal Atmos. Chem. Phys.
Discussion started: 22 May 2018

Atmospheric Chemistry and Physics Discussions

the lower stratosphere south of 60°S, the Merapi eruption contributed about 8800 tons of sulfur to the Antarctic lower stratosphere. This indicates that the long-range transport under favorable meteorological conditions enables tropical volcanic eruptions to be an important remote source of sulfur for the Antarctic stratosphere.

1 Introduction

Over the past two decades, multiple volcanic eruptions injected sulfur into the upper troposphere and lower stratosphere, which has been the dominant source of the stratospheric sulfate aerosol load (Vernier et al., 2011), preventing true background levels from other sources ever being seen (Solomon et al., 2011). Stratospheric sulfate aerosol mainly reflects solar radiation and absorbs infrared radiation, causing cooling of the troposphere and heating of the stratosphere. It contributes to the largest uncertainties to estimates and interpretations of the Earth's changing energy budget (Boucher et al., 2013). Further, by modulating the stratospheric and tropospheric temperature it has an impact on stratospheric dynamics, e. g. it can lead to dramatic phase changes of the quasi-biennial oscillation (Aquila et al., 2014) and alter the spatiotemporal characteristics of the El Niño–Southern Oscillation (ENSO) on both short (few years) and long (decades) timescales (Pausata et al., 2015). Stratospheric sulfate aerosol also has an impact on chemical processes in the lower stratosphere (Jäger and Wege, 1990; Solomon et al., 1993), in particular on polar ozone depletion (Tilmes et al., 2008; Drdla and Müller, 2012; Solomon et al., 2016). The presence of H_2SO_4 in the polar stratosphere in combination with cold temperatures facilitates the formation of polar stratospheric clouds (PSCs), which increase heterogeneous ozone depletion chemistry (Solomon et al., 1999; Zuev et al., 2015). Recent healing of Antarctic ozone depletion was constantly disturbed by moderate volcanic eruptions (Solomon et al., 2016). Mid- and high latitude explosive volcanic eruptions may directly influence the polar stratosphere. For example, the aerosol plume from the Calbuco eruption in 2015, including various volcanic gases, penetrated the polar vortex and caused a new record of the size of the Antarctic ozone hole after the eruption (Solomon et al., 2016; Ivy et al., 2017; Stone et al., 2017).

Usually, Antarctica is relatively free of local aerosol sources, but aerosols from low latitudes can reach Antarctica through long-range transport (Sand et al., 2017). Some of the sulfate found in the ice cores can be attributed to volcanic eruptions (Mazzera et al., 2001; Gao et al., 2007; Sigl et al., 2015). Measurements of enhanced aerosol in the lower Antarctic stratosphere right above the tropopause were made in October/November 1983, 84 and 85. These enhanced aerosol number concentrations were

attributed to aerosol transported to Antarctica from the eruption of the tropical volcano El Chichon in 1982 (Hofman and Rosen, 1985; Hofmann et al., 1988). Tropical volcanic eruptions can also enhance polar aerosols by long-range transport. Model results indicate that numerous moderate eruptions have affected ozone distributions over Antarctica, including the Merapi tropical eruption in October 2010 (Solomon et al., 2016). However, the transport mechanism is not well represented in present global climate models, and the uncertainties in modeled AOD in both polar regions are large (Sand et al., 2017).

The Mount Merapi (7.5°S, 110.4°E, elevation: 2930 m) is an active stratovolcano located in Central Java, Indonesia. Merapi has a long record of eruptive activities. The most recent large eruption with a volcanic explosivity index (VEI) of 4 occurred between 26 October and 7 November 2010 (Pallister et al., 2013), with SO_2 emission rates being a few orders of magnitude higher than previous eruptions. Following the Merapi eruption in 2010, evidence of poleward transport of sulfate aerosol towards southern hemisphere high latitudes was found in time series of aerosol observations by the Michelson Interferometer for Passive Atmospheric Sounding (MIPAS) (Günther et al., 2017) and Cloud-Aerosol Lidar with Orthogonal Polarization (CALIOP) (Khaykin et al., 2017) .

There are three main ways for transport out of the tropical tropopause layer (TTL): the deep and shallow branches of the Brewer-Dobson circulation (BDC) and horizontal mixing (Vogel et al., 2011). There is considerable year-to-year seasonal variability in the amount of irreversible transport from the tropics to high latitudes, which is related to both the phase of the QBO and the state of the polar vortex (Olsen et al., 2010). The BDC plays a large role in determining the distributions of many constituents in the extratropical lower stratosphere. And the faster quasi-horizontal transport between the tropics and polar regions also significantly contributes to determining these distributions. The efficiency of transporting constituents quasi-horizontally depends on wave breaking patterns and varies with time of year (Kravitz and Robock, 2011; Wu et al., 2017). Better knowledge of the transport pathways and an accurate representation of volcanic sulfur injections into the upper troposphere and lower stratosphere (UTLS) are key elements for understanding the global stratospheric aerosol budget is key to understanding the cooling effects and ozone loss linked to volcanic activity.

The aim of the present study is to investigate the quasi-horizontal transport by tracing the volcanic plume of the Merapi eruption from the tropics to Antarctica and quantifying its contribution to the sulfur load in the Antarctic lower stratosphere. In Sect. 2, the new Atmospheric Infrared Sounder (AIRS) SO_2 observations (Hoffmann et al., 2014), the MIPAS aerosol observations (Griessbach et al., 2016) and the method for reconstructing the SO_2 injection time series of the Merapi eruption are introduced. In

Sect. 3 the results are presented: first, the reconstructed time series of the Merapi eruption is discussed; second, the dispersion of the Merapi plume is investigated using up to 6 months long Lagrangian forward trajectories initialized with the reconstructed SO_2 time series; third, the simulation is compared to MIPAS volcanic aerosol measurements and the plume dispersion is investigated using MIPAS aerosol detections. In Sect.4 the results are discussed with the background of the meteorological conditions and conclusions are given in Sect. 5.

2 Satellite data, model and method

2.1 MIPAS instrument and aerosol measurements

MIPAS (Fischer et al., 2008) is an infrared limb emission spectrometer aboard the European Space Agency's (ESA's) Envisat, which provided nearly 10 years of measurements from July 2002 to April 2012. MIPAS spectral measurements cover the wavelength range from 4.15 to 14.6 microns. The vertical coverage of MIPAS' nominal measurement mode during the so-called `optimized resolution phase' from January 2005 to April 2012 was 7–72 km. The field of view of MIPAS was about 3 km × 30 km (vertically × horizontally) at the tangent point. The extent of the measurement volume along the line of sight was about 300 km, and the horizontal distance between two adjacent limb scans was about 500 km. On each day, ~14 orbits with ~90 profiles per orbit were measured. The vertical sampling was 1.5 km in the UTLS and 3 km above the UTLS. In 2010 and 2011, MIPAS measured for 4 days in nominal mode followed alternately by one day in middle atmosphere mode or upper atmosphere mode. In this study, we focussed on measurements in the nominal mode.

For the aerosol detections, we used the MIPAS altitude-resolved aerosol-cloud-index (ACI) products as introduced by Griessbach et al. (2016) to compare with the MPTRAC simulations and analyze the poleward transport of the Merapi volcanic plume. Small ACI values indicate large aerosol extinction coefficients and vice versa. For instance, MIPAS data points with ACI < 7 can cover infrared extinction coefficients larger than 1×10^{-4} km^{-1}, which corresponds to 3×10^{-4} km^{-1} in the visible wavelength range (Griessbach et al. 2016). Larger ACI values will show aerosol load with even smaller extinction coefficients. As ice clouds usually have extinction coefficients larger than 1×10^{-4} km^{-1}, we applied a brightness-temperature-correlation method, that serves as an ice cloud filter, to all MIPAS spectra with ACI<7 (Griessbach et al., 2016) to remove the ice clouds from the data set. The resulting aerosol product is be sensitive to different types of aerosol, in particular, volcanic ash, sulfate aerosol, mineral dust, as well as non-ice PSCs.

Atmos. Chem. Phys. Discuss., https://doi.org/10.5194/acp-2018-332
Manuscript under review for journal Atmos. Chem. Phys.
Discussion started: 22 May 2018

Atmospheric Chemistry and Physics Discussions

2.2 AIRS

AIRS (Aumann et al., 2003) is an infrared nadir sounder with across-track scanning capabilities aboard the National Aeronautics and Space Administration's (NASA's) Aqua satellite. Aqua was launched in 2002 and operates in a nearly polar Sun-synchronous orbit at about 710 km with a period of 98 min. AIRS provides nearly continuous measurement coverage with 14.5 orbits per day and with a swath width of 1780 km it covers the globe almost twice a day. The AIRS footprint size is 13.5 km × 13.5 km at nadir and 41 km × 21.4 km for the outermost scan angles respectively. The along-track distance between two adjacent scans is 18 km. The AIRS observations provide good horizontal resolution and make it ideal for observing the fine filamentary structures of volcanic SO_2 plumes.

In this study, we use an optimized SO_2 index (SI, unit: K) to estimate the amount of SO_2 injected into the atmosphere by the Merapi eruption 2010. The SI is defined as the brightness temperature differences in the 7.3 μm SO_2 waveband.

$$SI = BT\left(1412.87 cm^{-1}\right) - BT\left(1371.52\ cm^{-1}\right), \quad (1)$$

where BT is the brightness temperature measured at wavenumber ν. This SI is more sensitive to low concentrations and performs better on suppressing background interfering signals than the SI provided in the AIRS operational data products. It is an improvement of the SI definition given by Hoffmann et al. (2014) by means of a better choice of the background channel (selecting 1412.87 cm^{-1} rather than 1407.2 cm^{-1}). The SI increases with increasing SO_2 column density and it is most sensitive to SO_2 at altitudes above 3-5 km. SO_2 injections into the lower troposphere are usually not detectable in the infrared spectral region because the atmosphere gets opaque due to the water vapor continuum. A detection threshold of 1 K was used in this study to identify the Merapi SO_2 injections. AIRS detected the Merapi SO_2 cloud from 3 November to 15 November 2010.

2.3 MPTRAC model and reconstruction of the volcanic SO_2 injection time series of the Merapi eruption

In this study, we used the highly scalable MPTRAC model to investigate the volcanic eruption event. In the MPTAC model, air parcel trajectories are calculated based on numerical integration using wind fields from global meteorological reanalyses (Hoffmann et al., 2016; Rößler et al., 2017). Diffusion is modeled by uncorrelated Gaussian random displacements of the air parcels with zero mean and standard deviations $\sigma_x = \sqrt{D_x \Delta t}$ (horizontally) and $\sigma_z = \sqrt{D_z \Delta t}$ (vertically). D_x and D_z are the horizontal and vertical diffusivities respectively, and Δt is the time step for the trajectory calculations. For the

Merapi simulation, D_x and D_z were set to 50 $m^2 s^{-1}$ and 0 $m^2 s^{-1}$ in the troposphere and 0 $m^2 s^{-1}$ and 0.1 $m^2 s^{-1}$ in the stratosphere, respectively. In addition, sub-grid scale wind fluctuations, which are particularly important for long-range simulations, are simulated by a Markov model (Stohl et al., 2005; Hoffmann et al., 2016). Loss processes of chemical species, SO_2 in our case, are simulated based on an exponential decay of the mass assigned to each air parcel. In the stratosphere a constant half lifetime of 7 days was assumed for SO_2. Considering that the Merapi eruption occurred in the humid tropics, with high concentration of hydroxyl radical, a half lifetime of 2.5 days was assumed for the troposphere.

To estimate the time- and altitude-resolved SO_2 injections, we follow the approach of Hoffmann et al. (2016) and Wu et al. (2017) and use backward trajectories calculated with the MPTRAC model together with AIRS SO_2 measurements. Observations from 3 to 7 November 2010 were used for estimating the SO_2 injection during the explosive eruption. Since the AIRS measurements do not provide altitude information, we established a column of air parcels at each AIRS SO_2 detection. The vertical range of the column was set to 0–25 km, covering the possible vertical dispersion range of the SO_2 plume in the first few days. The AIRS footprint size varies between 14 and 41 km, hence in the horizontal direction, we chose an average of 30 km as the full width at half maximum (FWHM) for the Gaussian scatter of the air parcels. In our simulation, a fixed total number of 100,000 air parcels was assigned to all air columns and the number of air parcels in each column was scaled linearly proportional to the SO_2 index. Then backward trajectories were calculated for all air parcels, and trajectories that were at least 2 days but no more than 5 days long and that passed the volcano domain were recorded as emissions of Merapi. The volcano domain was defined by means of a search radius of 75 km around the location of the Merapi and 0–20 km in the vertical direction, covering all possible injection heights. Sensitivity experiments have been conducted to optimize these pre-assigned parameters to obtain the best simulation results. Our estimates of the Merapi SO_2 injection are shown in Sect. 3.

Starting with the reconstructed altitude-resolved SO_2 injection time series, the transport of the Merapi plume is simulated for 6 months, covering the time period from the initial eruption on 26 October 2010 to 30 April 2011. The trajectory calculations are driven by the ERA–Interim data (Dee et al., 2011) interpolated on a 1°× 1° horizontal grid on 60 model levels with the vertical range extending from the surface to 0.1 hPa. The ERA–Interim data are provided at 00, 06, 12 and 18 UTC. Outputs of model simulations are given every 3 hours at 00, 03, 06, 09, 12, 15, 18 and 21 UTC. The impact of different meteorological analysis on MPTRAC simulations was assessed by Hoffmann et al. (2016, 2017). In both studies the ERA–Interim data showed good performance.

Atmos. Chem. Phys. Discuss., https://doi.org/10.5194/acp-2018-332
Manuscript under review for journal Atmos. Chem. Phys.
Discussion started: 22 May 2018

3 Results

Figure 1 displays the time-latitude section of MIPAS aerosol detections with median ACI value in each bin smaller than 7 and within the vertical range of 13 and 20 km, covering the tropical tropopause layer (TTL) and the extratropical lowermost stratosphere (LMS). The MIPAS data captured all the major events that contributed to the aerosol load in the UTLS, i.e., moderate volcanic eruptions from 2002 to 2012 and one large bushfire in 2009, as well as the subsequent dispersion and change of aerosol load over time. Particularly, after the Merapi eruption in 2010, marked by the red triangle in Fig. 1, the MIPAS data show an obvious poleward transport of aerosol from the tropics to Antarctica.

3.1 Merapi eruption and SO_2 injection time series

According to the chronology of the Merapi eruption (Surono et al., 2012), the explosive eruption first occurred between 10:00 and 12:00 UTC on 26 October and this eruption generated a plume that reached 12 km altitude. A period of relative small explosive eruptions continued from 26 October to 31 October. During the initial period of the dome growth (1–3 November), the level of SO_2 degassing was relatively low compared with the SO_2 degassing before 1 November. On 3 November, the eruptive intensity increased again accompanied by much stronger degassing and a series of explosions. The intermittent explosive eruptions occurred during 4–5 November with the climactic eruption on 4 November, producing an ash column that reached up to 17 km altitude. From 6 November, explosive activity decreased slowly and the degassing declined.

Figure 2 shows the time- and altitude-resolved SO_2 injections of the Merapi eruption retrieved using the AIRS SO_2 index data and the backward-trajectory approach. It successfully reproduced the chronology of the Merapi eruption as outlined by Surono et al. (2012). Significant SO_2 was injected into altitudes below 8 km during the initial explosive eruptions on 26–30 October. Starting from 30 October the plume reached up to 12 km. During 1–3 November the SO_2 injections into altitudes below 12 km continued but the mass was less than in the initial phase. On 3 November the intensity increased again and peaked in the climactic explosive eruptions of 4–5 November. Before 3 November the reconstruction indicates a minor fraction of SO_2 right above the tropopause.

To study the long-range transport of the Merapi plume, we initialized 100,000 air parcels at the SO_2 injection time series shown in Fig. 2 with a SO_2 mass of 0.44 Tg as provided in Surono et al. (2012) and calculated forward trajectories for 6 months. Here, we only considered the plume in the upper troposphere and stratosphere where the lifetime of both SO_2 and sulfate aerosol is longer than that in the lower troposphere. Further, the SO_2 was all converted into sulfate aerosol within a few weeks (von

Glasow et al., 2009; we could also see it in the AIRS SO_2 and MIPAS aerosol data), and we assumed that the sulfate aerosol converted from SO_2 remains collocated with the SO_2 plume, i.e., the sedimentation of small sulfate aerosol particles was negligible for the timescale considered.

Figure 3 shows the evolution of the simulated Merapi plume and compares the plume altitudes to the aerosol top altitudes measured by MIPAS between 7 and 23 November. Immediately after the eruption, the majority of the plume moved towards the southwest and was entrained by the anticyclonic circulation of the tropical cyclone Anggrek (not shown). After the Anggrek weakened and dissipated, the majority of the plume parcels in upper troposphere moved eastward and those in the lower stratosphere moved westward. In general, the altitudes of the simulated plume are comparable to the MIPAS observations. The remaining discrepancies of air parcel altitudes being higher than the altitudes of MIPAS aerosol detections can be attributed to the fact that the MIPAS tends to underestimate aerosol top cloud altitudes, which is about 0.9 km in case of low extinction aerosol layers and can reach down to -4.5 km in case of broken cloud conditions (Höpfner et al., 2009).

3.2 Meteorological background conditions after the Merapi eruption

The Merapi eruption in October 2010 occurred during the seasonal transition from austral spring to summer when the polar vortex typically weakens and the ozone hole shrinks. As depicted in Fig. 4, the meteorological conditions at the polar lower stratosphere (150hPa, ~12km) after the eruption deviated from the climatological mean. The minimum temperature south of 50°S (Fig. 4a) was much lower than the climatological mean during mid-November to mid-December but still higher than the low temperature necessary for existence of PSCs. The polar mean temperature in Fig. 4b, defined as the temperature averaged over latitudes south of 60°S, stayed lower than the climatological mean from November 2010 until February 2011. Corresponding to the low temperatures, the average zonal wind speed at 60°S (Fig. 4c) was significantly larger than the climatological mean value from November 2010 to mid-January 2011. The eddy heat flux in Fig. 4d is the product of meridional wind departures and temperature departures from the respective zonal mean values. A more negative value of eddy heat flux indicates that wave systems are propagating into the stratosphere and are warming the polar region. There is a strong anticorrelation between temperature and the 45-day average of the eddy heat flux lagged prior to the temperature. Comparing with the climatological mean state, the polar vortex was more disturbed during mid-July to end of August. But from mid-October to late November, the heat flux was much smaller than the long-term average, which meant a reduction in dynamical disturbances of the polar vortex as the QBO changed into a strong westerly phase. Considering the temperature, the

subpolar wind speed and the heat flux, the polar vortex was colder and stronger in November and December 2010 compared with the same time in other years. The study of Klekociuk et al. (2011) also confirmed that the polar vortex area was consistently larger than the climatological mean particularly during November and December (see their Fig. 9). Consistent with the strength of the polar vortex, in November and December 2010 the ozone hole area in Fig. 4e, defined as the region of ozone values below 220 Dobson Units (DU) located south of 40°S, was larger than the climatological mean. Meanwhile, the low polar mean temperature and stable polar vortex resulted in a long-lasting ozone hole, which disappeared in the last week of December. The polar vortex broke down by mid-January 2011 when subpolar wind speed decreased below 15 m/s (Fig. 4c).

The poleward transport from the tropics to the polar region is known to be modulated by the phase of the quasi-biennial oscillation (QBO) and the state of the polar vortex itself: Fig. 4f shows that just before the Merapi eruption in 2010, the QBO switched from easterly phase to westerly phase. The westerly phase of the QBO promotes meridional transport from the tropics to subtropics, especially into the winter hemisphere (O'Sullivan and Dunkerton, 1997; Shuckburgh et al., 2001; Jäger, 2005). However, it also results in zonal wind acceleration at the high latitudes (Watson and Gray, 2014; Holton and Tan, 1980) and a less dynamically disturbed polar vortex (Anstey and Shepherd, 2014; Baldwin and Dunkerton, 1999), which will make it less possible for air parcels to penetrate the polar vortex.

3.3 Lagrangian simulation and satellite observation of poleward transport of the Merapi plume

The early plume evolution until about one month after the initial eruption is shown on the maps in Fig. 3 together with MIPAS observations of volcanic aerosol (only aerosol detections with ACI<7 are shown). Within about one month after the initial eruption, the plume was nearly entirely transported around the globe in the tropics, moving west at altitudes of about 17 km. The lower part of the plume, below about 17 km was transported south-eastward and reached latitudes south of 30°S by mid-November. The simulated long-term transport of the Merapi plume is illustrated in Fig. 5, showing the relative number of air parcels reaching a latitude-altitude bin every half a month. To verify the model results, the poleward transport of aerosols as detected by MIPAS is shown in Fig. 6. For comparison, only simulation results above the minimum altitude of MIPAS aerosol detections in Fig. 6 are shown in Fig. 5. In this study, we only focus on aerosol distributions in the upper troposphere and stratosphere, where sulfate aerosol has a longer lifetime and potential climate impacts.

During the first month after the eruption (Figs. 5a–b), the majority of the plume was transported southward roughly along the isentropic surfaces. The most significant pathway is above the core of the

subtropical jet in the southern hemisphere. However, because of the transport barrier of the polar jet during austral spring, the plume was confined to the north of 60°S. In December 2010 (Figs. 5c–d), a larger fraction of the plume was transported southward above the subtropical jet core, and deep into the polar region south of 60°S as the polar jet broke up. Till the end of January 2011, the majority of the plume had entered the mid- and high latitudes in the southern hemisphere, whereas only a very small proportion of the plume was transported north of 30°N. Substantial quasi-horizontal poleward transport from the TTL towards the LMS in Antarctica was found from November 2010 to February 2011 (Figs. 5a–h), approximately between 350 and 480 K (~10–20 km). From March to April 2011(Figs. 5i–l), the proportion of the plume that went across 60°S stopped increasing and the maxima of the plume descended from 380 to 350 K. During this transport towards Antarctica, a secondary upward transport split from the plume, which was particularly observable from January 2011 till the end of the simulation in April 2011(Figs. 5e–l). This slow upward transport was mainly located around 15°S above the tropopause and can be attributed to the upward branch of the BDC.

The poleward transport in the MPTRAC simulations was confirmed by MIPAS aerosol detections. MIPAS ACI zonal median values are shown in Fig. 6 for all MIPAS measurements after filtering out ice clouds. Small ACI values indicate a large aerosol load and large ACI values indicate clear air. As seen in Fig. 6, the locally confined aerosol plume from the Merapi eruption did not dominate the zonal median during the first half month after the eruption (Fig. 6a), but became evident between 350 and 380 K around the latitude of 7.5°S by the end of November (Fig. 6b) as the plume was transported around the globe in the tropics. As shown in the MPTRAC simulations, the transport towards the northern mid- and high latitudes was suppressed by the strong subtropical jets. The transport of the volcanic plume towards Antarctica in the UTLS region was observed from December 2010 to February 2011 (Figs. 6c–h) consistent with the simulations. The MIPAS aerosol data also demonstrated the upward transport from the tropical upper troposphere to the stratosphere, which was observed after late January 2010. The aerosol transported upward had increased the aerosol load in the tropical stratosphere reservoir compared to the aerosol load before the Merapi eruption.

Fig. 6 verified aerosol transport from the tropics to Antarctica and upward into the tropical stratosphere. However, before the eruption of Merapi, the aerosol load in the tropical stratosphere was already elevated by several small and moderate-size volcanic eruptions, namely the Sarychev Peak (12 Jun 2009), Nyamuragira (20 Jan 2010), Soufriere Hills (11 Feb 2010) and Pacaya (28 May 2010). In order to infer the increase of the aerosol load due to the eruption of Merapi from the MIPAS data, we calculated the median ACI between 1–4 November 2010 when there was no aerosol from the Merapi

eruption, to define the "background" aerosol load and then remove this "background" from the median ACI in Fig. 6. The results shown in Fig.7 demonstrate the change of median ACIs in the tropics and southern hemisphere corresponding to the same time period as Fig. 6, with positive/negative values indicating an increase/decrease of aerosol load. No significant change was observed during the first half month after the eruption due to the zonal averaging degrading the aerosol signal (Fig. 7a). The largest increase first appeared in the upper troposphere directly above Mount Merapi (Fig. 7b) and then moved quasi-horizontally southward into the UTLS region to ~40°S (Figs. 7c–f), consistent with what Figs. 5 and 6 showed. A relatively small but still significant increase of aerosol south of 60°S in the tropopause region was found from January 2011 (Fig. 7e) and it lasted until mid- April 2011 (Fig. 7j). Six months after the eruption, the aerosol levels were still slightly elevated in the tropical upper troposphere above 350 K. There should have been a decrease of the aerosol load in the tropical stratosphere because of sedimentation and poleward transport of aerosol if there were no aerosol from the Merapi eruption. But the upward transport of the Merapi aerosol compensated the loss.

3.4 Efficiency of quasi-horizontal transport from the tropics to Antarctica

As the results of the Lagrangian transport simulations with the MPTRAC model were comparable to the MIPAS observations (Sect. 3.3), it was possible not only to demonstrate the transport pathways but also to estimate the efficiency of the transport. The MPTRAC simulations and the MIPAS observations have demonstrated transport on the "surf zone" that reaches from the subtropics to high latitudes (Holton et al., 1995), where air masses are affected by both fast meridional transport and the slow BDC. Our data show that quasi-horizontal mixing in the lower extratropical stratosphere between 350 and 480 K is the main transport pathway for the volcanic aerosol. Figure 8 illustrates how the volcanic plume between 350 and 480 K approached Antarctica over time. Gray dashed and solid lines mark potential vortices (PV) contours with the largest PV gradients on the 350 and 480 K isentropic surfaces. These dynamically relevant PV contours represent horizontal transport barriers for air masses on the respective isentropic surface. On isentropic surfaces below 380 K, the contours of maximum PV gradients represent the dynamical discontinuity near the core of the subtropical jet stream and thus represent a transport barrier between the tropics and midlatitudes (Haynes and Shuckburgh, 2000; Kunz et al., 2011a,b). Isentropic transport of air masses across these boundaries indicates exchange between the tropics and extratropics due to Rossby wave breaking. On isentropic surfaces above 400 K, the contours of maximum PV gradients represent a boundary in the lower stratosphere, in particular, due to the polar vortices in winter (Kunz et al., 2015). For comparison we have also shown contour lines of ozone

column density of 220 DU (black isolines in Fig. 8), indicating the location and size of the ozone hole. The PV boundary on 480 K is in most cases collocated with the area of the ozone hole, showing that both quantities provide a consistent representation of the area of the polar vortex.

The Merapi volcanic plume first reached the 350 K transport boundary in mid-November and went close to the 480 K transport boundary in December. The long-lasting polar vortex prevented the volcanic plume from crossing the transport boundary in the beginning of December, but from mid-December, the polar vortex became more disturbed and displaced from the south pole, together with a shrinking ozone hole. As mentioned in Sect.3.2, the ozone hole broke up at the end of December 2010 and the polar vortex broke down by mid-January 2011.

The fractions of the volcanic plume that crossed the individual transport boundaries or the latitude of 60°S on each isentropic surface are shown in Fig. 9. In both cases, the proportion increased from November 2010 to January 2011. In November and December 2010 the largest plume transport across the transport boundaries occurred between the 360 and 430 K isentropic surface (Fig. 9a), with a peak at 380–390 K. In January and February 2011 the peak was slightly elevated to 390–400 K. In November 2010, the volcanic plume did not cross the 480 K transport boundary of the polar vortex at high altitudes, especially above about 450 K. The high-latitude fraction kept increasing from December 2010 to February 2011 as the weakening of the polar vortex made the transport boundary more permeable. In March and April 2011, the total proportion decreased and the peak descended to 370 K in March and further to 360 K in April. The proportion of the volcanic plume south of 60°S (Fig. 9b) increased slightly from November to December 2010, and then increased significantly from December 2010 to January and February 2011 at all altitudes as the polar vortex displaced and broke down. Finally, the transport to south of 60°S started to decrease in March 2011. From November 2010 to February 2011 the peak was around 370–400 K, but in March and April 2011 the peak resided around 350–370 K.

Figure 10 summarizes the poleward transport of the volcanic plume between 350 and 480 K. The zonally resolved fractions derived from the Lagrangian MPTRAC simulations and the fraction of air parcels south of 60°S are shown in Fig. 10a. Figure 10b demonstrates the increasing and decreasing aerosol load in this vertical range for MIPAS aerosol detections relative to 1–4 November median (see Sect.3.3). The poleward transport trend in Fig. 10a is comparable to the poleward migration of the enhanced aerosol in Fig. 10b. The simulations show that the plume reached 60°S by the end of November 2010. Correspondingly, the aerosol load south of 60°S was elevated when the volcanic plume was transported there. The percentage fluctuated, but increased until the end of February 2011, with a maximum percentage of about 4%. A steep increase occurred from mid-December 2010 to end of

January 2011, following the displacement and breakdown of the polar vortex. The elevated aerosol load south of 60°S decreased from March 2011, because the plume descended to altitudes below 350 K as shown by Fig. 9b. Overall, enhanced aerosol due to Merapi eruption was observed mostly in the subtropics and midlatitudes, but the aerosol load in the south polar region was also significantly elevated for three months from December 2010 to February 2011.

4 Discussion

The results presented in Sect. 3 show that the meridional transport of the Merapi volcanic plume to Antarctica mostly occurred between the isentropic surfaces of 350 and 480 K (about 10 to 20 km), covering the TTL and the lower stratosphere at mid- and high latitudes. For this long-range transport on timescales of a few months, fast isentropic transport associated with quasi-horizontal mixing was found to be the most efficient pathway. The phase of QBO, subtropical Rossby wave breaking and the strength and stability of the polar vortex all have an impact on the transport efficiency. The Merapi eruption occurred in austral spring and fast poleward transport was facilitated by the weakening subtropical jet and active Rossby wave breaking events. The westerly QBO enhanced transport and mixing in the subtropics with implications on the position of the subtropical barrier (Shuckburgh et al., 2001; Palazzi et al., 2011). The QBO also modulated the ability of upward propagating planetary waves to influence the strength of the polar vortex. Although the polar vortex was relatively stable when the Merapi eruption occurred, after the volcanic plume reached the south polar region, the polar vortex was displaced from the south pole and distorted because more wave systems propagated into the polar stratosphere and warmed the polar region, so that the volcanic plume could be transported from the tropics deep into Antarctica under all these favourable conditions.

The phase of the QBO influences the amount of volcanic emissions transported out of tropics, while the heating effect of a large amount of sulfur injected by volcanic eruptions can change the pattern of the QBO (Niemeier and Schmidt, 2017). With increasing emission rates the velocity of the equatorial jet streams increases and less sulfate is transported out of the tropics. The amount of SO_2 injected during the Merapi eruption 2010 was 0.44 Tg, far less than the 8 TgS/yr required to shut down or reverse the QBO pattern (Niemeier and Schmidt, 2017), so that the westerly phase of the QBO that promote meridional transport was under minor influence of the heating effect of sulfur in this case.

Based on the simulations in Sect. 3.4, up to ~4% of air parcels composed of SO_2 and sulfate aerosol were transported from the TTL to the lower stratosphere in the south polar region till the end of

February 2011, which means the Merapi eruption contributed about 8800 tons of sulfur to the polar lower stratosphere within 4 months after the eruption, assuming that the sulfate aerosol converted from SO_2 remained in the plume. In the lower stratosphere, the atmosphere is relatively dry and clean compared with the lower troposphere, so the sulfate aerosols may have a smaller chance to interact with clouds or to be washed out. In fact, in the polar lower stratosphere usually sedimentation and downward transport by the BDC are the main removal processes. Clouds and washout processes usually cannot be expected in the lower stratosphere. However, the amount of sulfate aerosols in the plume could also be affected by other mechanisms that speed up the loss of sulfur, for example, coagulation in the volcanic plume, the absorption of sulfur onto fine ash particles etc. But for a moderate eruption, such as the Merapi eruption, sulphuric particle growth may not be as significant as it is in a large volcanic eruption, so the scavenging efficiency of sulfur will be low.

Besides, a kinematic trajectory model like MPTRAC, in which reanalysis vertical wind is used as vertical velocity, typically shows higher vertical dispersion in the equatorial lower stratosphere compared with a diabatic trajectory model (Schoeberl et al., 2003; Wohltmann and Rex, 2008; Liu et al., 2010; Ploeger et al., 2010, 2011). However, the ERA–Interim reanalysis data used in this study to drive the model may constrain the vertical dispersion much better than older reanalyses (Liu et al., 2010; Hoffmann et al., 2017). The meridional transport in this study was mainly quasi-horizontal transport in the mid- and high latitude UTLS region, so the effect of the vertical speed scheme is limited. Meanwhile, the MIPAS aerosol detections confirmed the MPTRAC simulations, so our results can be considered as a representative value.

The aerosol transported to the polar lower stratosphere will finally descend with the downward flow in the polar region to lower altitudes, and have a chance to become a nonlocal source of sulfur for Antarctica by dry and wet deposition, following the general precipitation patterns. Quantifying the sulfur deposition flux onto Antarctica is beyond the scope of this study, though. Model results of Solomon et al. (2016) suggest that the Merapi eruption made a small but significant contribution to ozone depletion over Antarctica in the vertical range of 200–100 hPa (~10–14 km). This altitude range is in agreement with our results, where we found transport into the Antarctic stratosphere between 10 and 20 km. When the volcanic plume was transported to Antarctica in December 2010, the polar synoptic temperature at these low height levels was already too high for the formation of PSCs. The additional ozone depletion found by Solomon et al. (2016) together with the fact that sulfate aerosol was transported from the Merapi into the Antarctic stratosphere between November and February where no PSCs are present during polar summer, may support the study which suggested that significant ozone

depletion can also occur on cold binary aerosol (Drdla and Müller, 2012). The Merapi eruption in 2010 could be an interesting case study for more sophisticated geophysical models to study the aftermath of volcanic eruptions on polar processes.

5 Summary and conclusion

In this study, we analyzed the poleward transport pathway and the transport efficiency of volcanic aerosol released by the Merapi eruption in October 2010 from tropics to the Antarctic lower stratosphere. The analysis was based on AIRS SO_2 measurements, MIPAS sulfate aerosol detections and MPTRAC transport simulations. First, we estimated altitude-resolved SO_2 injection time series during the explosive eruption period using AIRS data together with a backward trajectory approach. Second, the long-range transport of the volcanic plume from the initial eruption to 30 April 2010 was simulated based on the derived SO_2 injection time series. Then the evolution and the poleward migration of the volcanic plume was analyzed and validated with MIPAS aerosol measurements.

Results of this study suggest that the volcanic plume from the Merapi eruption was transported from the tropics to south of 60°S within a time scale of one month. Later on a significant fraction of the volcanic plume crossed 60°S, even further to Antarctica until the end of February 2011. As a result, the aerosol load in the Antarctic lower stratosphere was significantly elevated for 3 months from December 2010 to February 2011. From March 2011, the aerosol transported to the polar lower stratosphere descended with the downward flow of the Brewer-Dobson circulation to lower altitudes. This relatively fast meridional transport and the distribution of volcanic aerosol was mainly carried out by quasi-horizontal mixing from the TTL to the extratropical lower stratosphere, which in turn was facilitated by the weakening of the subtropical jet in the seasonal transition from austral spring to summer. Based on the simulations, the most efficient pathway for this quasi-horizontal mixing occurred between isentropic surfaces of 360 to 430 K. The polar vortex in late austral spring 2010 was relatively strong compared to the climatological mean state. However, when the plume went to the south polar region, the polar vortex was displaced off the south pole, so that the volcanic plume was able to enter to the south pole without even penetrating the polar vortex.

Overall, after the Merapi eruption, the largest increase of aerosol load occurred in the southern hemisphere midlatitudes and a relatively small but significant fraction of the volcanic plume (4%) was further transported to the Antarctic lower stratosphere within 4 months after the eruption. This contributed 8800 tons of sulfur to the Antarctic stratosphere, which indicates that long-range transport

under favorable meteorological conditions enables tropical volcanic eruptions to be an important remote source of sulfur to Antarctica.

Code and data availability. AIRS data are distributed by the NASA Goddard Earth Sciences Data Information and Services Center. The SO_2 index data used in this study (Hoffmann et al., 2014) are available for download at https://datapub.fz-juelich.de/slcs/airs/volcanoes/ (last access: 17 December 2017). Envisat MIPAS Level-1B data are distributed by the European Space Agency. The ERA–Interim reanalysis data (Dee et al., 2011) were obtained from the European Centre for Medium-Range Weather Forecasts. The code of the Massive-Parallel Trajectory Calculations (MPTRAC) model is available under the terms and conditions of the GNU General Public License, Version 3 from the repository at https://github.com/slcs-jsc/mptrac (last access: 31 December 2017).

Competing interests. The authors declare that they have no conflict of interest.

Acknowledgments. This work was supported by National Natural Science Foundation of China under grant no. 41605023 and International Postdoctoral Exchange Fellowship Program 2015 under grant no. 20151006.

Reference

Anstey, J. A., and Shepherd, T. G.: High-latitude influence of the quasi-biennial oscillation, Q. J. R. Meteorol. Soc., 140, 1-21, doi: 10.1002/qj.2132, 2014.

Aquila, V., C. I. Garfinkel,P.A.Newman, L. D. Oman, and D. W. Waugh, Modifications of the quasi-biennial oscillation by a geoengineering perturbation of the stratospheric aerosol layer, Geophys. Res. Lett., 41, 1738-1744, doi: 10.1002/2013GL058818, 2014.

Aumann, H. H., Chahine, M. T., Gautier, C., Goldberg, M. D., Kalnay, E., McMillin, L. M., Revercomb, H., Rosenkranz, P. W., Smith, W. L., Staelin, D. H., Strow, L. L., and Susskind, J.: AIRS/AMSU/HSB on the Aqua mission: design, science objectives, data products, and processing systems, IEEE Trans. Geosci. Remote Sens., 41, 253-264, doi: 10.1109/TGRS.2002.808356, 2003.

Baldwin, M. P., and Dunkerton, T. J.: Propagation of the Arctic Oscillation from the stratosphere to the troposphere, J. Geophys. Res. Atmos., 104, 30937-30946, doi: 10.1029/1999JD900445, 1999.

Dee, D. P., Uppala, S. M., Simmons, A. J., Berrisford, P., Poli, P., Kobayashi, S., Andrae, U., Balmaseda, M. A., Balsamo, G., Bauer, P., Bechtold, P., Beljaars, A. C. M., van de Berg, L., Bidlot, J., Bormann, N., Delsol, C., Dragani, R., Fuentes, M., Geer, A. J., Haimberger, L., Healy, S. B., Hersbach, H., Holm, E. V., Isaksen, L., Kallberg, P., Kohler, M., Matricardi, M., McNally, A. P., Monge-Sanz, B. M., Morcrette, J. J., Park, B. K., Peubey, C., de Rosnay, P., Tavolato, C., Thepaut, J. N., and Vitart, F.: The ERA-Interim reanalysis: configuration and performance of the data assimilation system, Q. J. R. Meteorol. Soc., 137, 553-597, doi: 10.1002/qj.828, 2011.

Drdla, K., and Müller, R.: Temperature thresholds for chlorine activation and ozone loss in the polar stratosphere, Ann. Geophys., 30, 1055-1073, doi: 10.5194/angeo-30-1055-2012, 2012.

Fischer, H., Birk, M., Blom, C., Carli, B., Carlotti, M., von Clarmann, T., Delbouille, L., Dudhia, A., Ehhalt, D., Endemann, M., Flaud, J. M., Gessner, R., Kleinert, A., Koopman, R., Langen, J., López-Puertas, M., Mosner, P., Nett, H., Oelhaf, H., Perron, G., Remedios, J., Ridolfi, M., Stiller, G., and Zander, R.: MIPAS: an instrument for atmospheric and climate research, Atmos. Chem. Phys., 8, 2151-2188, doi: 10.5194/acp-8-2151-2008, 2008.

Gao, C., Oman, L., Robock, A., and Stenchikov, G. L.: Atmospheric volcanic loading derived from bipolar ice cores: Accounting for the spatial distribution of volcanic deposition, J. Geophys. Res. Atmos., 112, D09109, doi: 10.1029/2006JD007461, 2007.

Griessbach, S., Hoffmann, L., Spang, R., von Hobe, M., Müller, R., and Riese, M.: Infrared limb emission measurements of aerosol in the troposphere and stratosphere, Atmos. Meas. Tech., 9, 4399-4423, doi:10.5194/amt-9-4399-2016, 2016.

Günther, A., Höpfner, M., Sinnhuber, B. M., Griessbach, S., Deshler, T., von Clarmann, T., and Stiller, G.: MIPAS observations of volcanic sulphate aerosol and sulphur dioxide in the stratosphere, Atmos. Chem. Phys. Discuss., 2017, 1-32, doi: 10.5194/acp-2017-538, 2017.

Haynes, P., and Shuckburgh, E.: Effective diffusivity as a diagnostic of atmospheric transport: 2. Troposphere and lower stratosphere, J. Geophys. Res. Atmos., 105, 22795-22810, doi: 10.1029/2000JD900092, 2000.

Heng, Y., Hoffmann, L., Griessbach, S., Rößler, T., and Stein, O.: Inverse transport modeling of volcanic sulfur dioxide emissions using large-scale simulations, Geosci. Model Dev., 9, 1627-1645, doi:10.5194/gmd-9-1627-2016, 2016.

Hoffmann, L., Griessbach, S., and Meyer, C. I.: Volcanic emissions from AIRS observations: detection methods, case study, and statistical analysis, in: Remote Sensing of Clouds and the Atmosphere XIX and Optics in Atmospheric Propagation and Adaptive Systems XVII, edited by: Comeron, A., Kassianov, E. I., Schafer, K., Picard, R. H., Stein, K., and Gonglewski, J. D., Proceedings of SPIE, Spie-Int Soc Optical Engineering, Bellingham, doi: 92421410.1117/12.2066326, 2014.

Hoffmann, L., Hertzog, A., Rößler, T., Stein, O., and Wu, X.: Intercomparison of meteorological analyses and trajectories in the Antarctic lower stratosphere with Concordiasi superpressure balloon observations, Atmos. Chem. Phys., 17, 8045-8061, doi: 10.5194/acp-17-8045-2017, 2017.

Hoffmann, L., Rößler, T., Griessbach, S., Heng, Y., and Stein, O.: Lagrangian transport simulations of volcanic sulfur dioxide emissions: Impact of meteorological data products, J. Geophys. Res. Atmos., 121, 4651-4673, doi: 10.1002/2015JD023749, 2016.

Hofmann, D. J., Rosen, J. M., and Gringel, W.: Delayed production of sulfuric acid condensation nuclei in the polar stratosphere from El Chichon volcanic vapors, Journal of Geophysical Research: Atmospheres, 90, 2341-2354, doi:10.1029/JD090iD01p02341, 1985.

Hofmann, D. J., Rosen, J. M., and Harder, J. W.: Aerosol measurements in the winter/spring Antarctic stratosphere: 1. Correlative measurements with ozone, Journal of Geophysical Research: Atmospheres, 93, 665-676, doi:10.1029/JD093iD01p00665, 1988.

Holton, J. R., Haynes, P. H., McIntyre, M. E., Douglass, A. R., Rood, R. B., and Pfister, L.: Stratosphere-troposphere exchange, Reviews of Geophysics, 33, 403-439, doi: 10.1029/95RG02097, 1995.

Holton, J. R., and Tan, H. C.: The Influence of the Equatorial Quasi-Biennial Oscillation on the Global Circulation at 50 mb, J. Atmos. Sci., 37, 2200-2208, doi: 10.1175/1520-0469(1980)037<2200:tioteq>2.0.co;2, 1980.

Höpfner, M., Pitts, M. C., and Poole, L. R.: Comparison between CALIPSO and MIPAS observations of polar stratospheric clouds, Journal of Geophysical Research: Atmospheres, 114, doi:10.1029/2009JD012114, 2009.

548 Ivy, D. J., Solomon, S., Kinnison, D., Mills, M. J., Schmidt, A., and Neely, R. R.: The influence of the
549 Calbuco eruption on the 2015 Antarctic ozone hole in a fully coupled chemistry-climate model,
550 Geophys. Res. Lett., 44, 2556-2561, doi: 10.1002/2016GL071925, 2017.
551 Jäger, H.: Long-term record of lidar observations of the stratospheric aerosol layer at
552 Garmisch-Partenkirchen, J. Geophys. Res. Atmos., 110, D08106, doi: 10.1029/2004JD005506, 2005.
553 Jäger, H., and Wege, K.: Stratospheric ozone depletion at northern midlatitudes after major volcanic
554 eruptions, J. Atmos. Chem., 10, 273-287, doi: 10.1007/bf00053863, 1990.
555 Khaykin, S. M., Godin-Beekmann, S., Keckhut, P., Hauchecorne, A., Jumelet, J., Vernier, J. P.,
556 Bourassa, A., Degenstein, D. A., Rieger, L. A., Bingen, C., Vanhellemont, F., Robert, C., DeLand,
557 M., and Bhartia, P. K.: Variability and evolution of the midlatitude stratospheric aerosol budget from
558 22 years of ground-based lidar and satellite observations, Atmos. Chem. Phys., 17, 1829-1845, doi:
559 10.5194/acp-17-1829-2017, 2017.
560 Klekociuk, A., Tully, M., Alexander, S., Dargaville, R., Deschamps, L., Fraser, P., Gies, H., Henderson,
561 S., Javorniczky, J., and Krummel, P.: The Antarctic ozone hole during 2010, Aust. Meteorol. Ocean.
562 Journal., 61, 253, 2011.
563 Kravitz, B., and Robock, A.: Climate effects of high-latitude volcanic eruptions: Role of the time of
564 year, J. Geophys. Res. Atmos., 116, D01105, 10.1029/2010JD014448, 2011.
565 Kunz, A., Konopka, P., Müller, R., and Pan, L. L.: Dynamical tropopause based on isentropic potential
566 vorticity gradients, J. Geophys. Res. Atmos., 116, D01110, doi: 10.1029/2010JD014343, 2011a.
567 Kunz, A., Pan, L. L., Konopka, P., Kinnison, D. E., and Tilmes, S.: Chemical and dynamical
568 discontinuity at the extratropical tropopause based on START08 and WACCM analyses, J. Geophys.
569 Res. Atmos., 116, D24302, doi: 10.1029/2011JD016686, 2011b.
570 Kunz, A., Sprenger, M., and Wernli, H.: Climatology of potential vorticity streamers and associated
571 isentropic transport pathways across PV gradient barriers, J. Geophys. Res. Atmos., 120, 3802-3821,
572 doi: 10.1002/2014jd022615, 2015.
573 Liu, Y. S., Fueglistaler, S., and Haynes, P. H.: Advection-condensation paradigm for stratospheric water
574 vapor, J. Geophys. Res. Atmos., 115,D24307, doi: 10.1029/2010JD014352, 2010.
575 Mazzera, D. M., Lowenthal, D. H., Chow, J. C., and Watson, J. G.: Sources of PM10 and sulfate aerosol
576 at McMurdo station, Antarctica, Chemosphere, 45, 347-356, doi:
577 https://doi.org/10.1016/S0045-6535(00)00591-9, 2001.
578 Niemeier, U., and Schmidt, H.: Changing transport processes in the stratosphere by radiative heating of
579 sulfate aerosols, Atmos. Chem. Phys., 17, 14871-14886, doi: 10.5194/acp-17-14871-2017, 2017.
580 Olsen, M. A., Douglass, A. R., Schoeberl, M. R., Rodriquez, J. M., and Yoshida, Y.: Interannual
581 variability of ozone in the winter lower stratosphere and the relationship to lamina and irreversible
582 transport, J. Geophys. Res.-Atmos., 115, 10.1029/2009jd013004, 2010.
583 O'Sullivan, D., and Dunkerton, T. J.: The influence of the quasi-biennial oscillation on global
584 constituent distributions, J. Geophys. Res. Atmos., 102, 21731-21743, doi: 10.1029/97JD01689,
585 1997.
586 Palazzi, E., Fierli, F., Stiller, G. P., and Urban, J.: Probability density functions of long-lived tracer
587 observations from satellite in the subtropical barrier region: data intercomparison, Atmos. Chem.
588 Phys., 11, 10579-10598, doi: 10.5194/acp-11-10579-2011, 2011.
589 Pallister, J. S., Schneider, D. J., Griswold, J. P., Keeler, R. H., Burton, W. C., Noyles, C., Newhall, C.
590 G., and Ratdomopurbo, A.: Merapi 2010 eruption—Chronology and extrusion rates monitored with
591 satellite radar and used in eruption forecasting, J. Volcanol. Geotherm. Res., 261, 144-152, doi:
592 http://dx.doi.org/10.1016/j.jvolgeores.2012.07.012, 2013.

Pausata, F. S. R., Chafik, L., Caballero, R., and Battisti, D. S.: Impacts of high-latitude volcanic eruptions on ENSO and Asian monsoon, Proceedings of the National Academy of Sciences, 112, 13784-13788, doi: 10.1073/pnas.1509153112, 2015.

Ploeger, F., Konopka, P., Gunther, G., Grooss, J. U., and Muller, R.: Impact of the vertical velocity scheme on modeling transport in the tropical tropopause layer, J. Geophys. Res. Atmos., 115, 14, doi: 10.1029/2009jd012023, 2010.

Ploeger, F., Fueglistaler, S., Grooss, J. U., Gunther, G., Konopka, P., Liu, Y. S., Muller, R., Ravegnani, F., Schiller, C., Ulanovski, A., and Riese, M.: Insight from ozone and water vapour on transport in the tropical tropopause layer (TTL), Atmos. Chem. Phys., 11, 407-419, doi: 10.5194/acp-11-407-2011, 2011.

Rößler, T., Stein, O., Heng, Y., and Hoffmann, L.: Regional and seasonal truncation errors of trajectory calculations using ECMWF high-resolution operational analyses and forecasts, Geosci. Model Dev. Discuss., 2017, 1-27, doi: 10.5194/gmd-2016-314, 2017.

Sand, M., Samset, B. H., Balkanski, Y., Bauer, S., Bellouin, N., Berntsen, T. K., Bian, H., Chin, M., Diehl, T., Easter, R., Ghan, S. J., Iversen, T., Kirkevåg, A., Lamarque, J. F., Lin, G., Liu, X., Luo, G., Myhre, G., Noije, T. V., Penner, J. E., Schulz, M., Seland, Ø., Skeie, R. B., Stier, P., Takemura, T., Tsigaridis, K., Yu, F., Zhang, K., and Zhang, H.: Aerosols at the poles: an AeroCom Phase II multi-model evaluation, Atmos. Chem. Phys., 17, 12197-12218, doi: 10.5194/acp-17-12197-2017, 2017.

Schoeberl, M. R., Douglass, A. R., Zhu, Z. X., and Pawson, S.: A comparison of the lower stratospheric age spectra derived from a general circulation model and two data assimilation systems, J. Geophys. Res. Atmos., 108, 16, doi: 10.1029/2002jd002652, 2003.

Shuckburgh, E., Norton, W., Iwi, A., and Haynes, P.: Influence of the quasi-biennial oscillation on isentropic transport and mixing in the tropics and subtropics, J. Geophys. Res. Atmos., 106, 14327-14337, doi: 10.1029/2000JD900664, 2001.

Sigl, M., Winstrup, M., McConnell, J. R., Welten, K. C., Plunkett, G., Ludlow, F., Buntgen, U., Caffee, M., Chellman, N., Dahl-Jensen, D., Fischer, H., Kipfstuhl, S., Kostick, C., Maselli, O. J., Mekhaldi, F., Mulvaney, R., Muscheler, R., Pasteris, D. R., Pilcher, J. R., Salzer, M., Schupbach, S., Steffensen, J. P., Vinther, B. M., and Woodruff, T. E.: Timing and climate forcing of volcanic eruptions for the past 2,500 years, Nature, 523, 543-549, doi: 10.1038/nature14565http://www.nature.com/nature/journal/v523/n7562/abs/nature14565.html#supplementary-information, 2015.

Solomon, S.: Stratospheric ozone depletion: A review of concepts and history, Reviews of Geophysics, 37, 275-316, doi: 10.1029/1999RG900008, 1999.

Solomon, S., Daniel, J. S., Neely, R. R., Vernier, J.-P., Dutton, E. G., and Thomason, L. W.: The Persistently Variable "Background" Stratospheric Aerosol Layer and Global Climate Change, Science, 333, 866-870, doi: 10.1126/science.1206027, 2011.

Solomon, S., Ivy, D. J., Kinnison, D., Mills, M. J., Neely, R. R., and Schmidt, A.: Emergence of healing in the Antarctic ozone layer, Science, doi: 10.1126/science.aae0061, 2016.

Solomon, S., Sanders, R. W., Garcia, R. R., and Keys, J. G.: Increased chlorine dioxide over Antarctica caused by volcanic aerosols from Mount-Pinatubo, Nature, 363, 245–248, doi: https://doi.org/10.1038/363245a0, 1993.

Stohl, A., Forster, C., Frank, A., Seibert, P., and Wotawa, G.: Technical note: The Lagrangian particle dispersion model FLEXPART version 6.2, Atmos. Chem. Phys., 5, 2461-2474, doi:10.5194/acp-5-2461-2005, 2005.

Stone, K. A., Solomon, S., Kinnison, D. E., Pitts, M. C., Poole, L. R., Mills, M. J., Schmidt, A., Neely, R. R., Ivy, D., Schwartz, M. J., Vernier, J.-P., Johnson, B. J., Tully, M. B., Klekociuk, A. R.,

König-Langlo, G., and Hagiya, S.: Observing the Impact of Calbuco Volcanic Aerosols on South Polar Ozone Depletion in 2015, J. Geophys. Res. Atmos., 122, 11,862-811,879, doi: 10.1002/2017JD026987, 2017.

Surono, Jousset, P., Pallister, J., Boichu, M., Buongiorno, M. F., Budisantoso, A., Costa, F., Andreastuti, S., Prata, F., Schneider, D., Clarisse, L., Humaida, H., Sumarti, S., Bignami, C., Griswold, J., Carn, S., Oppenheimer, C., and Lavigne, F.: The 2010 explosive eruption of Java's Merapi volcano—A '100-year' event, J. Volcanol. Geotherm. Res., 241, 121-135, doi: http://dx.doi.org/10.1016/j.jvolgeores.2012.06.018, 2012.

Tilmes, S., Muller, R., and Salawitch, R.: The sensitivity of polar ozone depletion to proposed geoengineering schemes, Science, 320, 1201-1204, doi: 10.1126/science.1153966, 2008.

Vernier, J. P., Thomason, L. W., Pommereau, J. P., Bourassa, A., Pelon, J., Garnier, A., Hauchecorne, A., Blanot, L., Trepte, C., Degenstein, D., and Vargas, F.: Major influence of tropical volcanic eruptions on the stratospheric aerosol layer during the last decade, Geophys. Res. Lett., 38, L12807, 10.1029/2011GL047563, 2011.

Vogel, B., Pan, L. L., Konopka, P., Gunther, G., Muller, R., Hall, W., Campos, T., Pollack, I., Weinheimer, A., Wei, J., Atlas, E. L., and Bowman, K. P.: Transport pathways and signatures of mixing in the extratropical tropopause region derived from Lagrangian model simulations, J. Geophys. Res.-Atmos., 116, 16, doi: 10.1029/2010jd014876, 2011.

von Glasow, R., Bobrowski, N., and Kern, C.: The effects of volcanic eruptions on atmospheric chemistry, Chem. Geol., 263, 131-142, doi: http://dx.doi.org/10.1016/j.chemgeo.2008.08.020, 2009.

Watson, P. A. G., and Gray, L. J.: How Does the Quasi-Biennial Oscillation Affect the Stratospheric Polar Vortex?, J. Atmos. Sci., 71, 391-409, doi: 10.1175/jas-d-13-096.1, 2014.

Wohltmann, I., and Rex, M.: Improvement of vertical and residual velocities in pressure or hybrid sigma-pressure coordinates in analysis data in the stratosphere, Atmos. Chem. Phys., 8, 265-272, doi: 10.5194/acp-8-265-2008, 2008.

Wu, X., Griessbach, S., and Hoffmann, L.: Equatorward dispersion of a high-latitude volcanic plume and its relation to the Asian summer monsoon: a case study of the Sarychev eruption in 2009, Atmos. Chem. Phys., 17, 13439-13455, doi: 10.5194/acp-17-13439-2017, 2017.

Zuev, V. V., Zueva, N. E., Savelieva, E. S., and Gerasimov, V. V.: The Antarctic ozone depletion caused by Erebus volcano gas emissions, Atmos. Environ., 122, 393-399, doi: https://doi.org/10.1016/j.atmosenv.2015.10.005, 2015.

Atmos. Chem. Phys. Discuss., https://doi.org/10.5194/acp-2018-332
Manuscript under review for journal Atmos. Chem. Phys.
Discussion started: 22 May 2018

Atmospheric Chemistry and Physics Discussions

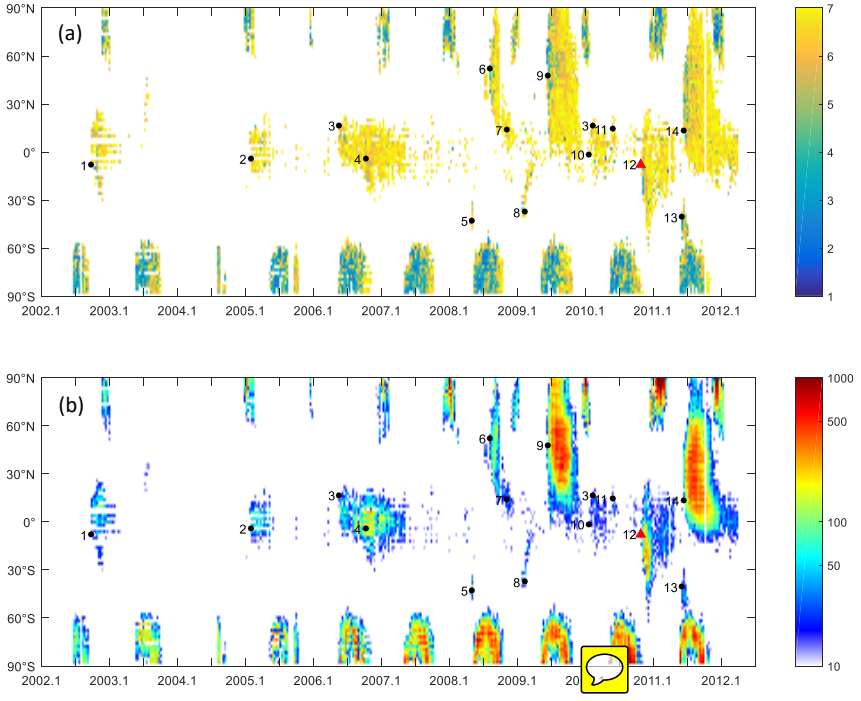

Figure 1: (a) Median value of ACI (ACI<7) and (b) number of MIPAS aerosol detections between 13 and 20 km (bin size 10 days and 2 ° in latitude). The red triangle indicates the eruption of Mount Merapi. The black dots indicate 1 Raung, 2 Manam, 3 Soufriere Hills, 4 Tavurvur (Rabaul), 5 Chaitén, 6 Kasatochi, 7 Dalaffilla, 8 Australian bushfire, 9 Sarychev Peak, 10 Nyamuragira, 11 Pacaya, 12 Mount Merapi, 13 Puyehue-Cordón Caulle, 14 Nabro.

Atmos. Chem. Phys. Discuss., https://doi.org/10.5194/acp-2018-332
Manuscript under review for journal Atmos. Chem. Phys.
Discussion started: 22 May 2018

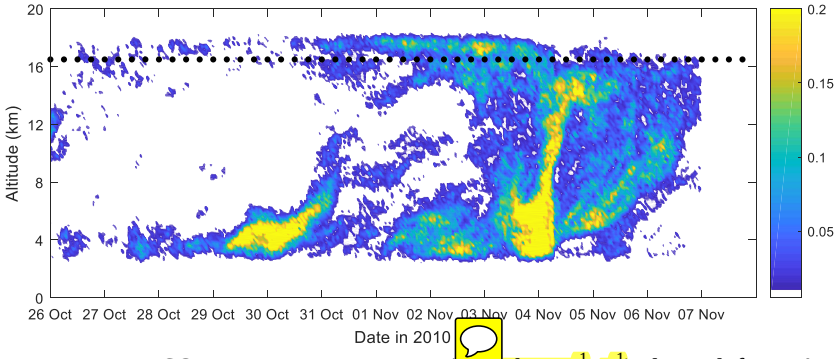

Figure 2: Merapi SO_2 emission time series (unit: kg m^{-1} s^{-1}) derived from AIRS measurements using a backward trajectory approach (see text for details). The emission data are binned every 1 h and 0.2 km. Gray dots denote the height of the thermal tropopause (based on the ERA–Interim reanalysis).

Atmos. Chem. Phys. Discuss., https://doi.org/10.5194/acp-2018-332
Manuscript under review for journal Atmos. Chem. Phys.
Discussion started: 22 May 2018

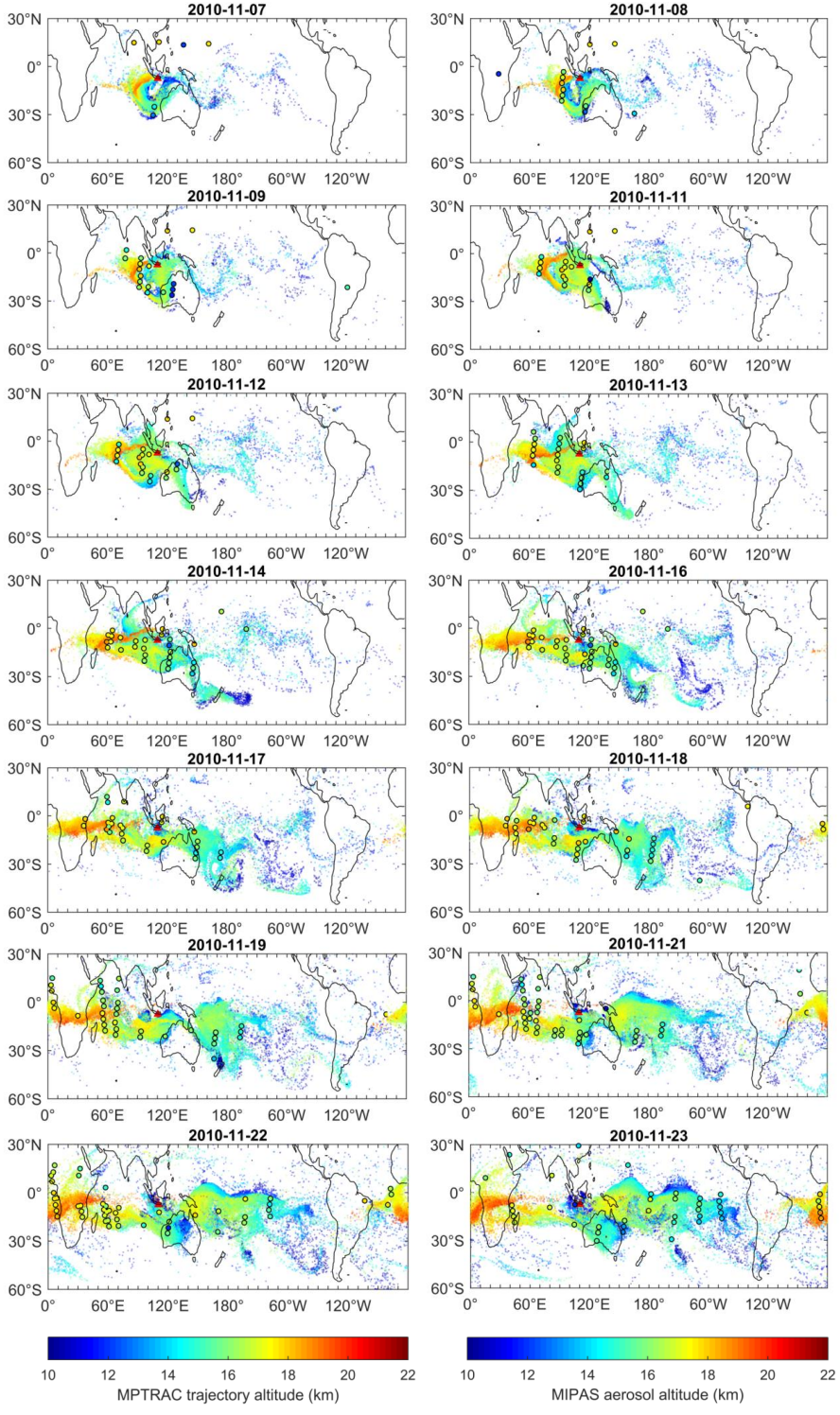

Figure 3: Distribution of the volcanic plume (showing only air parcels higher than 10 km, shading) from MPTRAC simulations (shown for 00:00UTC on selected days) and MIPAS aerosol detections (ACI < 7) within ±6 h (color-filled circles). The altitudes of all

air parcels, regardless of their SO_2 values, are shown. The red triangle denotes the location of Mount Merapi.

Atmos. Chem. Phys. Discuss., https://doi.org/10.5194/acp-2018-332
Manuscript under review for journal Atmos. Chem. Phys.
Discussion started: 22 May 2018

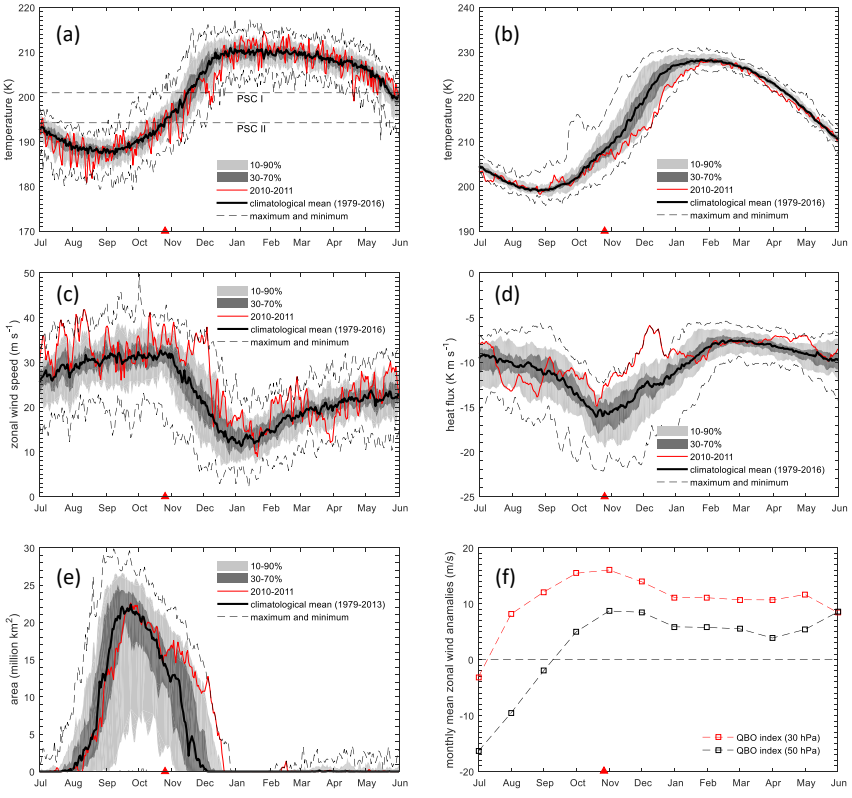

Figure 4: (a) Minimum temperature south of 50 ℃S at 150 hPa; (b) temperature averaged over the polar cap for latitudes south of 60 ℃S at 150 hPa; (c) zonal wind speed at 60 ℃S at 150 hPa; (d) eddy heat flux averaged between 45 ℃S and 75 ℃S for the 45-day period prior to the date indicated at 150 hPa; (e) ozone hole area from July 2010 to May 2011; (f) monthly mean zonal wind anomalies at 30 and 50 hPa. Temperatures for PSC existence in (a) are determined by assuming a nitric acid concentration of 6 ppbv and a water vapor concentration of 4.5 ppmv. (a)–(e) are based on MERRA2 data and (f) is based on NCEP/NCAR reanalysis. The ozone hole area in (e) is determined from OMI ozone satellite measurements. The red triangles indicate the time of the Merapi eruption.

Atmos. Chem. Phys. Discuss., https://doi.org/10.5194/acp-2018-332
Manuscript under review for journal Atmos. Chem. Phys.
Discussion started: 22 May 2018

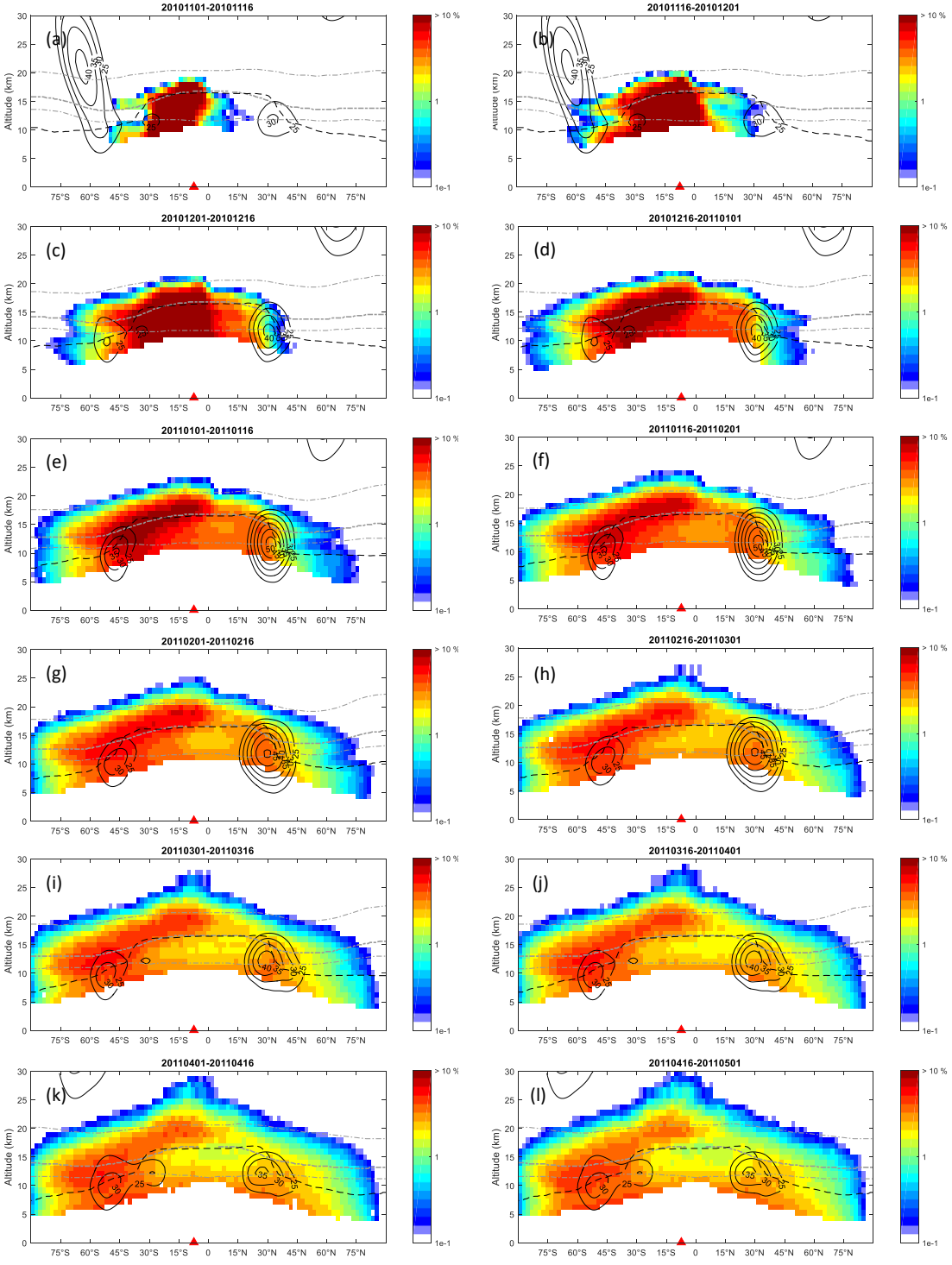

Figure 5: Percentage (%) of air parcels in proportion to the total number of air parcels from MPTRAC simulations, overlapped with monthly mean zonal winds (black contours), the thermal tropopause (black dashed line), the 380 K potential temperature isoline (thick gray dashed line) and 350 and 480 K potential temperature isolines (thin gray dashed lines). Results

are binned every 2 °in latitude and 1 km in altitude. The red triangle denotes the latitude of the Merapi. Please see title of each figure for the time period covered.

Atmos. Chem. Phys. Discuss., https://doi.org/10.5194/acp-2018-332
Manuscript under review for journal Atmos. Chem. Phys.
Discussion started: 22 May 2018

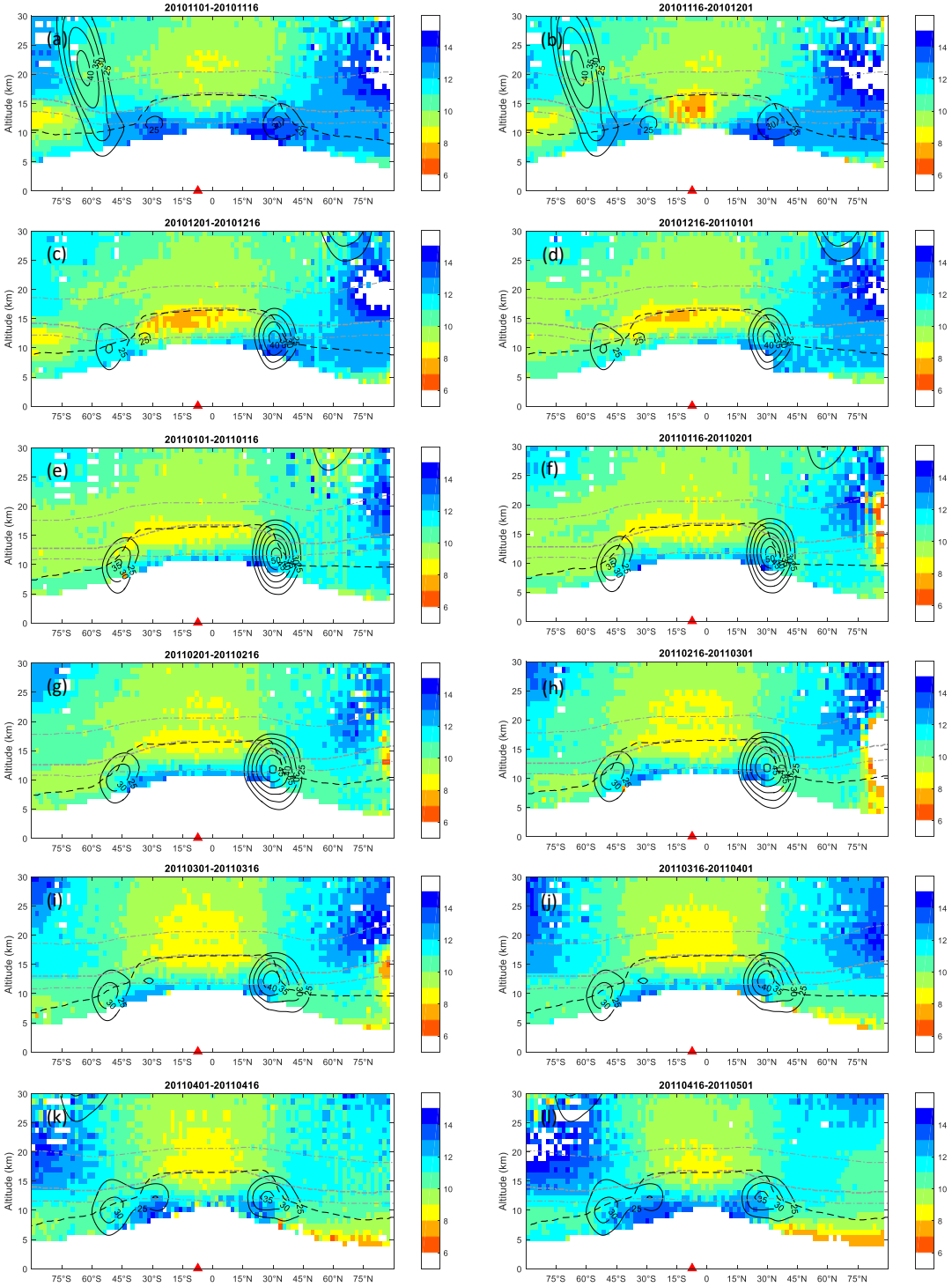

Figure 6: Median value of ACI of MIPAS aerosol detections (ice clouds filtered out), overlapped with monthly mean zonal winds (black contours), the thermal tropopause (black dashed line), the 380 K potential temperature isoline (thick gray dashed line) and 350 and 480 K potential temperature isolines (thin gray dashed lines). Results are binned

Atmos. Chem. Phys. Discuss., https://doi.org/10.5194/acp-2018-332
Manuscript under review for journal Atmos. Chem. Phys.
Discussion started: 22 May 2018

Atmospheric Chemistry and Physics Discussions

every 2 °in latitude and 1 km in altitude. Only median ACI values of 5–15 are shown. The red triangle denotes the latitude of the Merapi. Please see title of each figure for the time period covered.

Atmos. Chem. Phys. Discuss., https://doi.org/10.5194/acp-2018-332
Manuscript under review for journal Atmos. Chem. Phys.
Discussion started: 22 May 2018

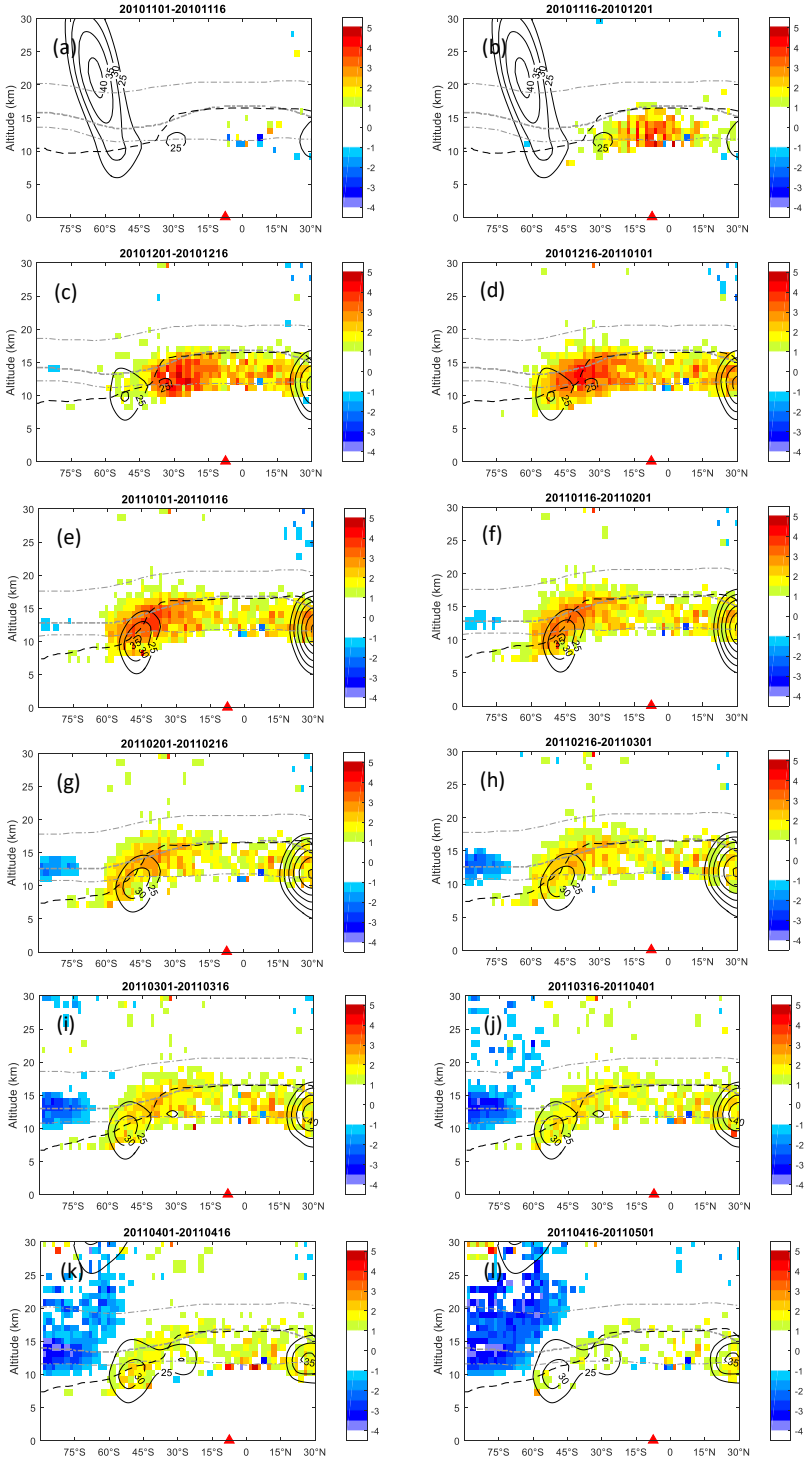

Figure 7: Change of aerosol load after the eruption of Merapi in 2010, overlapped with monthly mean zonal winds (black contours), the thermal tropopause (black dashed line), the 380 K potential temperature isoline (thick gray dashed line) and 350 and 480 K potential temperature isolines (thin gray dashed lines). Results are binned every 2 ° in

latitude and 1 km in altitude. The red triangle denotes the latitude of the Merapi. Please see title of each figure for the time period covered.

Atmos. Chem. Phys. Discuss., https://doi.org/10.5194/acp-2018-332
Manuscript under review for journal Atmos. Chem. Phys.
Discussion started: 22 May 2018

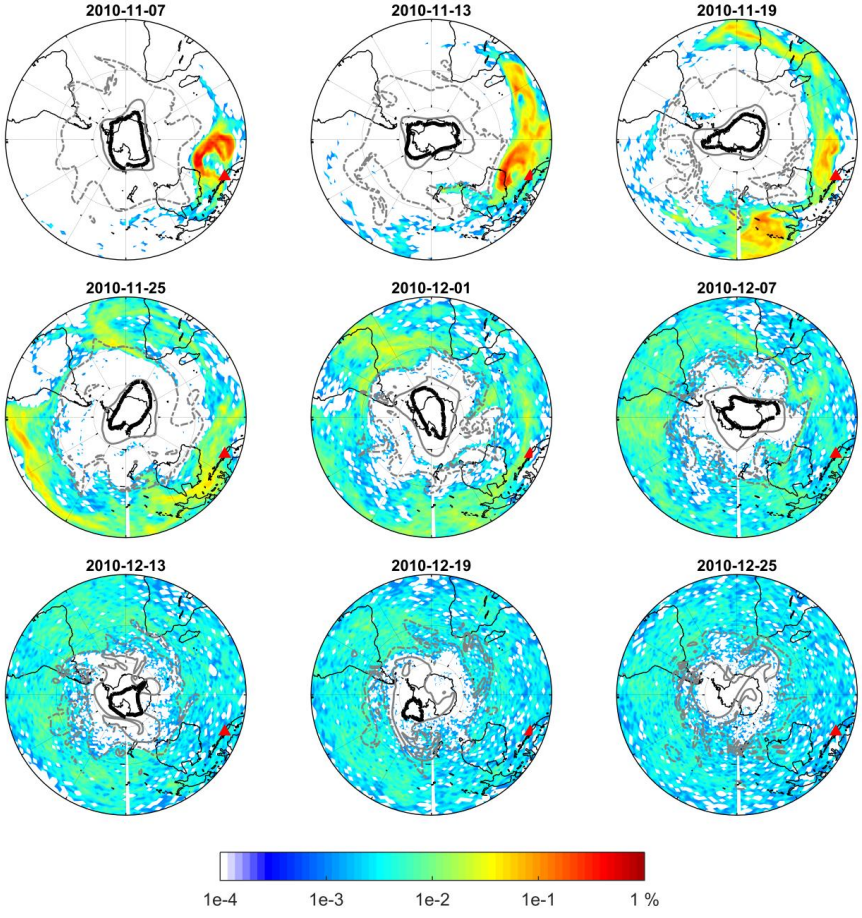

Figure 8: Percentage (%) of air parcels between the isentropic surfaces of 350 and 480 K in proportion to the total number of air parcels initialized in the Lagrangian transport simulation, at 12:00 UTC on selected dates. Results are binned every 2 ° in longitude and 1 ° in latitude. The black contour indicates OMI daily mean ozone column density of 220 DU. PV contours marked with gray dashed and solid lines show transport boundaries on the 350 and 480 K isentropic surfaces respectively (Kunz et al., 2015). The red triangle denotes the location of Mount Merapi

Atmos. Chem. Phys. Discuss., https://doi.org/10.5194/acp-2018-332
Manuscript under review for journal Atmos. Chem. Phys.
Discussion started: 22 May 2018

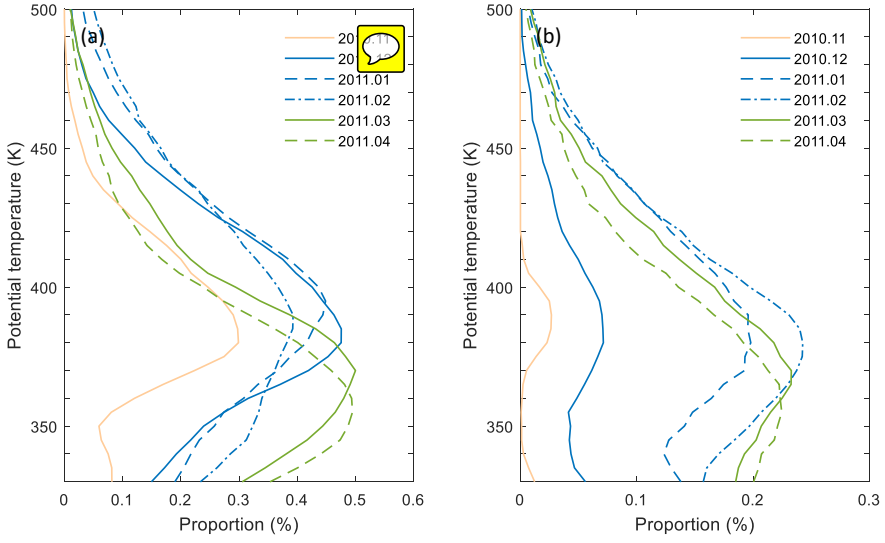

Figure 9: (a) Proportion (%) of the air parcels poleward of the PV-based transport boundaries at the end of each month; (b) proportion (%) of the air parcels south of 60 ℃S.

Atmos. Chem. Phys. Discuss., https://doi.org/10.5194/acp-2018-332
Manuscript under review for journal Atmos. Chem. Phys.
Discussion started: 22 May 2018

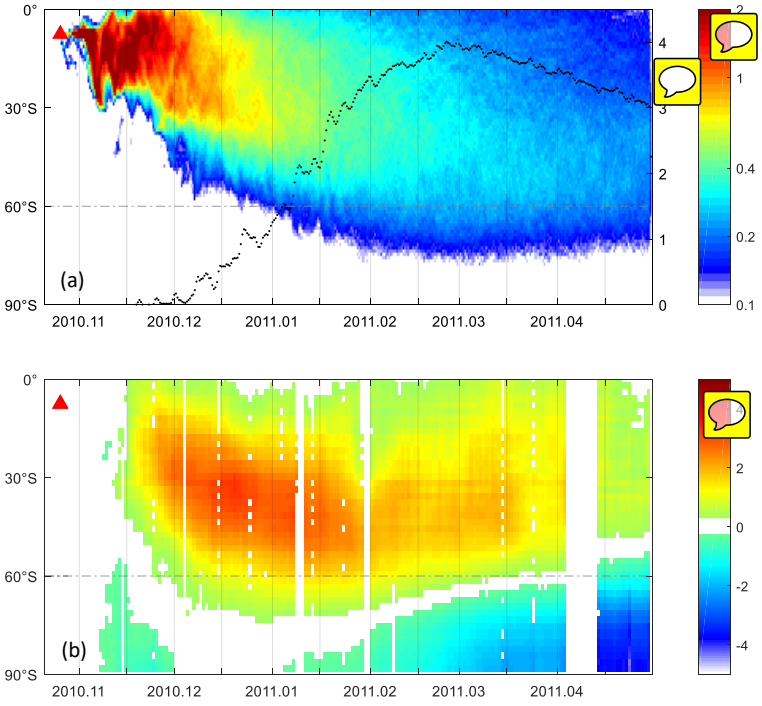

Figure 10: (a) Percentage (%) of air parcels between 350 and 480 K from MPTRAC simulations (shading, only percentages larger than 0.1% are shown; bin size: 12h and 1 ° in latitude), overlapped with proportion (%) of air parcels south of 60 °S (black dots); (b) Change of measured aerosol load between 350 and 480 K. Positive/negative values indicate increase/decrease of aerosol (bin size: 24h and 1 °in latitude). The red triangle denotes the time and latitude of the Merapi eruption